JOURNAL OF GUIDANCE, CONTROL, AND DYNAMICS
Vol. 29, No. 3, May–June 2006

# Predictive Optimal Control of a Hyperbolic Distributed Model for a Wind Tunnel

Nhan Nguyen*
*NASA Ames Research Center, Moffett Field, California 94035*
and
Mark Ardema†
*Santa Clara University, Santa Clara, California 95053*

**A new optimal-control approach is described, based on first-order hyperbolic partial differential equations to investigate a Mach number control problem for a closed-circuit wind tunnel. The flow in the wind tunnel is modeled as a distributed system using the Euler equations and is controlled by a compressor at the system boundary. The control inputs to the compressor are in turn controlled by a lumped-parameter system modeled by ordinary differential equations that represent dynamics of a drive-motor system and an inlet guide vane system. Optimality conditions of these coupled distributed and lump-parameter systems are developed using variational principles to establish an adjoint formulation for the optimal-control problem. The results are applied to a design of a predictive linear-quadratic optimal control for stabilizing the Mach number during a disturbance in the wind tunnel.**

## Nomenclature

| | | |
|---|---|---|
| $A$ | = | cross-sectional area |
| $\boldsymbol{A}, \boldsymbol{B}$ | = | hyperbolic system matrices |
| $A_m, L_m$ | = | test model reference area and length |
| $b, d, r$ | = | compressor empirical coefficients |
| $\boldsymbol{C}, \boldsymbol{D}, \boldsymbol{E}, \boldsymbol{F}$ | = | lumped-parameter linear system matrices |
| $C_D$ | = | drag coefficient |
| $\boldsymbol{C}_e, \boldsymbol{Q}_e, \boldsymbol{S}, \boldsymbol{U}$ | = | Hamiltonian system matrices |
| $c$ | = | speed of sound |
| $D$ | = | hydraulic diameter |
| $e$ | = | internal energy |
| $f$ | = | Darcy–Weisbach friction factor |
| $\boldsymbol{f}$ | = | state transition function |
| $\boldsymbol{G}, H$ | = | linear boundary condition matrix and coefficient |
| $\boldsymbol{g}$ | = | boundary condition function |
| $H_1, H_2, H_3$ | = | Hamiltonian functions |
| $J$ | = | cost function |
| $K_a, K_m$ | = | drive-motor torque constants |
| $K_c, K_v, K_\theta$ | = | inlet guide vane system constants |
| $k$ | = | specific heat ratio |
| $L$ | = | duct length |
| $L_s, R_s$ | = | drive-motor stator inductance and resistance |
| $L_1, L_2$ | = | cost-weighting functions |
| $M$ | = | Mach number |
| $\dot{m}$ | = | mass flow |
| $n, n^-$ | = | numbers of eigenvalues and negative eigenvalues |
| $P, \boldsymbol{Q}, \boldsymbol{R}$ | = | linear-quadratic cost-weighting factors |
| $p$ | = | static pressure |
| $q$ | = | forcing function |
| $R_r$ | = | drive-motor rotor resistance control |
| $T$ | = | static temperature |
| $t$ | = | time |
| $t_d$ | = | time delay |
| $t_f$ | = | final time |
| $t_L$ | = | time period |
| $u$ | = | flow speed |
| $\boldsymbol{u}$ | = | lumped-parameter state vector |
| $V_a$ | = | inlet guide vane field voltage control |
| $\boldsymbol{v}$ | = | control vector |
| $\boldsymbol{W}, \boldsymbol{V}$ | = | Riccati equation matrices |
| $w$ | = | disturbance function |
| $x$ | = | position coordinate |
| $x_t$ | = | position coordinate of test section |
| $\boldsymbol{y}$ | = | distributed state vector |
| $\alpha, \beta$ | = | linear advection equation coefficients |
| $\gamma$ | = | time-horizon parameter |
| $\Delta$ | = | perturbation |
| $\delta$ | = | variation |
| $\boldsymbol{\eta}$ | = | boundary-condition adjoint vector |
| $\theta$ | = | inlet guide vane flap deflection |
| $\lambda$ | = | eigenvalue, distributed adjoint variable |
| $\boldsymbol{\lambda}$ | = | distributed adjoint vector |
| $\boldsymbol{\mu}$ | = | lumped-parameter adjoint vector |
| $\xi$ | = | compressor-speed error integral |
| $\rho$ | = | static density |
| $\tau$ | = | time to go |
| $\chi$ | = | distance to go |
| $\omega$ | = | compressor speed |
| $\omega_s$ | = | drive-motor synchronous speed |

*Subscript*

| | | |
|---|---|---|
| 0 | = | stagnation condition |

*Superscripts*

| | | |
|---|---|---|
| $L$ | = | evaluated at $x = L$ |
| $T$ | = | matrix transpose operation |
| 0 | = | evaluated at $x = 0$ |

Received 3 January 2005; revision received 3 May 2005; accepted for publication 4 May 2005. 

*Research Scientist, Mail Stop 269-1, Intelligent Systems Division. Member AIAA.

†Professor, Department of Mechanical Engineering. Associate Fellow AIAA.

## Introduction

IN THIS PAPER, we present a new optimal-control approach for a distributed system governed by first-order hyperbolic partial differential equations (PDEs) coupled with a lumped-parameter system modeled by ordinary differential equations (ODEs) imposed at the distributed system boundary. A system is called distributed if its state variable is not only time dependent but also spatially

dependent. Such a system has many physical applications such as coordinated control of a large quantity of multiple vehicles; for example, a Eulerian air-traffic-control model.[1] Optimal control of distributed systems modeled by PDEs is an active area of mathematical research in optimization theories. A large body of literature exists, contributed by many authors such as Fursikov et al.,[2] Raymond and Zidani,[3] and Troltzsch[4] in recent years. However, the focus of this research has been mostly on abstract mathematics that usually cannot be readily applied to a control design. Conversely, practical control engineering is still largely based on a lumped-parameter assumption. In some instances, lumped-parameter models are actually reduced from finer-scaled models that are governed by PDEs. For example, Inman describes distributed control of a flexible structure based on a lumped-parameter model resulting from a modal transformation of the Euler–Bernoulli beam equation.[5] Thus, a need exists for application-oriented optimal-control theories for distributed systems that serve as a bridge between pure mathematics of optimization research and practical control engineering. The goal of this paper is to present such an optimal-control theory and its application to solving a Mach number control problem for a wind tunnel using a distributed-system approach based on hyperbolic equations that model many physical systems governed by conservation laws such as fluids, elastodynamics, and traffic flow.

Wind tunnels are used for testing flight vehicles and are important tools for aircraft and space-flight vehicle design. The majority of wind tunnels are of a closed-circuit configuration. Air flow in these wind tunnels is recirculated through a closed-circuit duct by a compressor to achieve a desired air speed in a test section for aerodynamic testing purposes. An example wind tunnel of this type is the NASA Ames 11 × 11-ft transonic wind tunnel (11-ft TWT).

Figure 1 illustrates the NASA Ames 11-ft TWT. It is capable of delivering an air speed from Mach 0.2 to Mach 1.5 in a test section 11 ft wide × 11 ft high. The air flow is delivered by a compressor driven by a set of synchronous-induction AC motors operated in a speed range from 310 to 645 rpm with a total input power of 236,000 hp. The compressor is a variable-geometry machine equipped with inlet guide vanes (IGVs) that have adjustable trailing-edge flaps with a range of angular deflections from −7.5 to 19.5 deg.

The test-section aerodynamic condition is normally controlled to ensure that the Mach number variation is within a prescribed tolerance, which can be as small as 0.001. For subsonic flow, the Mach number control is accomplished by adjusting the IGV flap deflection at a fixed compressor speed as shown in Fig. 2.

During a Mach number control, a motor-drive-speed control system regulates the compressor speed set points at all times to avoid operation near critical speeds of rotor-blade resonances. Thus, the flow condition as well as the compressor speed must be controlled simultaneously. The current Mach number control is strictly a feedback scheme as shown in the block diagram in Fig. 3.

Typically, during a wind-tunnel test, the test model is pitched through a series of angles of attack (AOA) at a nominal Mach number. This is known as a pitch polar. As the AOA increases, the drag force on the test model also increases. This drag force translates into a loss in the total pressure across the test model. The total pressure disturbance then propagates downstream to the compressor inlet and sets up a dynamic imbalance in the compressor equilibrium, thereby causing the compressor speed to fall. This consequently results in a deviation in the Mach number in the test section from the desired set

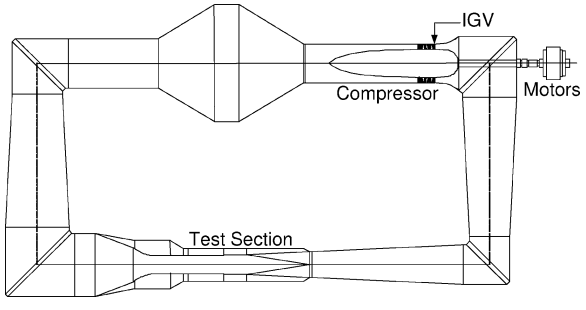


**Fig. 1 NASA Ames 11 × 11-ft transonic wind tunnel.**

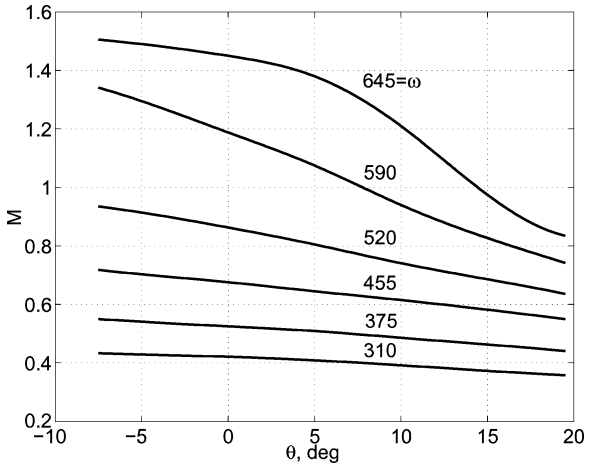


**Fig. 2 NASA Ames 11-ft TWT Mach envelope.**

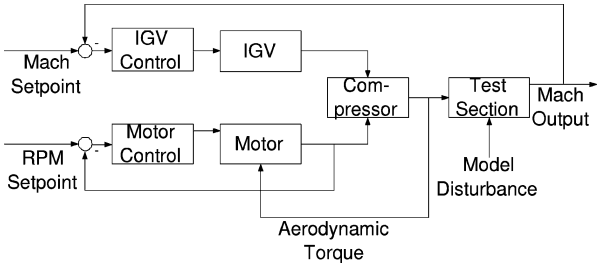


**Fig. 3 NASA Ames 11-ft TWT Mach number control.**

point. To minimize this Mach number deviation, the test model has to be paused in between changes in the pitch angle so that the flow condition can be reestablished by a Mach number feedback control using the IGVs.

It is a recognized that the current Mach number control strategy can be further improved by allowing the test model to be actuated continuously while the Mach number is actively regulated to maintain its set point. This would translate into a significant advantage over the current pitch-pause mode. Therefore, the motivation of this study is to investigate an improved predictive Mach number feedforward control for a wind tunnel based on a framework of optimal control of distributed systems modeled by hyperbolic equations.

## Wind-Tunnel Control Modeling

Modeling of flow in a duct or a wind tunnel for control-design purposes using fluid-dynamics equations has rarely been considered because of the inherent complexity in dealing with partial differential equations. Understandably, many wind-tunnel control models have been based on heuristic or ad hoc methods. Soeterboek[6] describes a method for control modeling of a test-section Mach number by an experimental transfer function coupled with a time delay. The current Mach number control for NASA Ames 11-ft TWT was developed using a quasi-steady-state model based on an empirical relationship between the Mach number and the compressor performance characteristics. The quasi-steady-state model circumvents the need for modeling the complex unsteady air flow but does not capture the time-delay effect. As a result, it can lead to poor control handling of disturbance rejection as a result of the test model drag-induced total pressure disturbance that exists in a typical wind tunnel.

## Distributed Model

To motivate a general discussion on optimal control for a distributed system, we propose to establish a distributed model of the wind-tunnel flow based on the governing laws of physics to capture the spatial dependency of the flow variables. In the process, this model should be more accurate than a heuristic model and thus can be used as a basis for the proposed predictive Mach number optimal-control study. The governing Euler equations for one-dimensional

flow are[7]

$$\frac{\partial}{\partial t}(\rho A)+\frac{\partial}{\partial x}(\rho u A)=0 \tag{1}$$

$$\frac{\partial}{\partial t}(\rho u A)+\frac{\partial}{\partial x}(pA+\rho u^2 A)-p\frac{dA}{dx}+\frac{1}{2}\rho u^2 A\frac{f}{D}=0 \tag{2}$$

$$\frac{\partial}{\partial t}\left(\rho eA+\frac{1}{2}\rho u^2 A\right)+\frac{\partial}{\partial x}\left(\rho ueA+\frac{1}{2}\rho u^3 A+puA\right)=0 \tag{3}$$

where $\rho$ is the static density, $u$ is the flow speed, $p$ is the static pressure, $e$ is the internal energy, $A$ is the cross-sectional area, $D$ is the hydraulic diameter, and $f$ is the friction factor.

Equations (1–3) are the conservation law of fluid flow. It is, however, usually more convenient to express these equations in terms of the mass flow $\dot{m}$, the total pressure $p_0$, and the total temperature $T_0$ because these variables can be measured directly from pressure and temperature sensors. We now introduce an alternate form of the Euler equations as follows:

$$\boldsymbol{y}_t+\boldsymbol{A}(\boldsymbol{y},x)\boldsymbol{y}_x+\boldsymbol{B}(\boldsymbol{y},x)=\boldsymbol{0} \tag{4}$$

where $\boldsymbol{y}(x,t)=[\dot{m}\ \ p_0\ \ T_0]^T$ is a distributed state vector and

$$\boldsymbol{A}=\begin{bmatrix} u & \dfrac{pA}{p_0} & \dfrac{\dot{m}u}{2T_0} \\ \dfrac{\rho_0 c^2}{\rho A} & u\left[1-\dfrac{(k-1)T}{T_0}\right] & \dfrac{\rho_0 c^2 u}{T_0} \\ \dfrac{(k-1)T}{\rho A} & -\dfrac{(k-1)^2 Tu}{kp_0} & u\left[1+\dfrac{(k-1)T}{T_0}\right] \end{bmatrix}$$

$$\boldsymbol{B}=\begin{bmatrix} \dfrac{\dot{m}uf}{2D} \\ \dfrac{kp_0u^3f}{2c^2D}\left[1-\dfrac{(k-1)T}{T_0}\right] \\ -\dfrac{(k-1)^2Tu^3f}{2c^2D} \end{bmatrix}$$

where $c$ is the speed of sound, $T$ is the static temperature, $\rho_0$ is the total density, and $k$ is the specific heat ratio.

Equation (4) is generally classified as a first-order, quasi-linear hyperbolic PDE system as determined by that fact that the matrix $\boldsymbol{A}$ possesses real and distinct eigenvalues. In fact, it can be shown that these eigenvalues are $u$ and $u\pm c$, which are the wave-propagation speeds in a fluid medium. Subsonic flow therefore involves two waves propagating downstream and one wave propagating upstream from the source.

The flow recirculation in a wind tunnel is controlled by a compressor, which creates a pressure rise to compensate for the pressure losses throughout the wind tunnel. Using the one-dimensional flow model, we let $x=0$ and $x=L$ correspond to the compressor exit and inlet stations, respectively. Then, the boundary conditions for Eq. (4) are specified by the following compressor-performance model, which can be obtained empirically from experimental data as

$$\dot{m}(0,t)=\dot{m}(L,t) \tag{5}$$

$$p_0(0,t)=\left[1+\sum_{i=2}^{4}\sum_{j=0}^{2}\frac{r_{ij}\theta^j\omega^i}{\sqrt{T_0^i(L,t)}}\right]\times\left[b_1p_0(L,t)-\frac{b_2\dot{m}(L,t)\sqrt{T_0(L,t)}}{\sum_{i=1}^{3}\sum_{j=0}^{2}\left[d_{ij}\theta^j\omega^i\Big/\sqrt{T_0^i(L,t)}\right]}\right] \tag{6}$$

$$T_0(0,t)=T_0(L,t)+\frac{b_2\omega}{\dot{m}(L,t)}[p_0(0,t)-p_0(L,t)] \tag{7}$$

where $b_i$, $d_{ij}$, and $r_{ij}$ are the empirical coefficients.

Equation (5) is the continuity equation, and Eqs. (6) and (7) are the respective momentum and energy equations that relate the total pressure and temperature rises across the compressor to the compressor speed $\omega$ and the IGV flap deflection $\theta$, which are the control inputs to the compressor.

As an important consideration for hyperbolic equations, boundary conditions must be well posed such that the numbers of incoming and outgoing boundary conditions are equal to number of positive and negative eigenvalues, respectively. Equations (5–7) satisfy this requirement for either subsonic flow, which requires two boundary conditions at $x=0$ and one boundary condition at $x=L$, or supersonic flow, which requires all three boundary conditions at $x=0$.

## Lumped-Parameter Model

As indicated, both the flow condition in the wind tunnel and the compressor speed must be controlled simultaneously. Therefore, we must take into account the dynamics of the drive motors and the IGV system that actually control the compressor speed and IGV flap deflection. The three-phase synchronous-induction AC drive motors use a liquid-rheostat system as a primary means of changing the rotor resistance $R_r$, which changes the motor torque to control the compressor speed. The dynamics of this drive-motor system is described by the following motor torque equation:

$$\dot{\omega}=\frac{K_mR_r\omega_s(\omega_s-\omega)}{[R_s(\omega_s-\omega)+R_r\omega_s]^2+L_s^2\omega_s^2(\omega_s-\omega)^2}-K_a[p_0(0,t)-p_0(L,t)] \tag{8}$$

where $R_s$ is the stator resistance, $L_s$ is the stator inductance, $\omega_s$ is the synchronous speed, and $K_m$ and $K_a$ are the torque constants.

The IGVs are driven by DC servo motors and controlled by the motor field voltage $V_a$. The dynamics of this system is modeled as

$$\dot{\theta}=K_vV_a-\tfrac{1}{2}\rho(L,t)u^2(L,t)(K_\theta\theta+K_c) \tag{9}$$

where $K_v$, $K_\theta$, and $K_c$ are the IGV system constants.

We observed that the control inputs $\omega$ and $\theta$ to the compressor become the states or outputs of the drive motors and the IGV system. Both Eqs. (8) and (9) also depend on the distributed flow variables at the boundary. Thus, Eqs. (8) and (9) are coupled with Eq. (4) through the boundary conditions in Eqs. (5–7).

## Validation

To validate the wind-tunnel distributed model, we compute a transition from Mach 0.6 at 455 rpm to Mach 0.9 at 590 rpm as shown in Figs. 4–6. The simulation is based on a computational fluid dynamics (CFD) numerical method using a flux-splitting, first-order upwind finite-difference explicit scheme[8] with the wind-tunnel distributed model discretized into 45 nodes. At each node, there are three flow quantities, and so the discretized model contains a total of 135 aerodynamic states plus two compressor dynamic states and two control inputs.

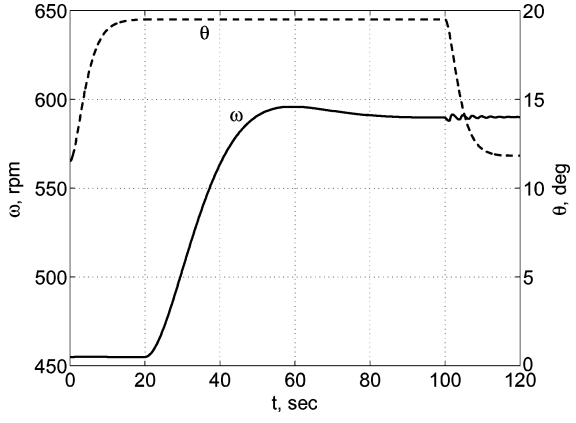


**Fig. 4 Compressor control time history.**

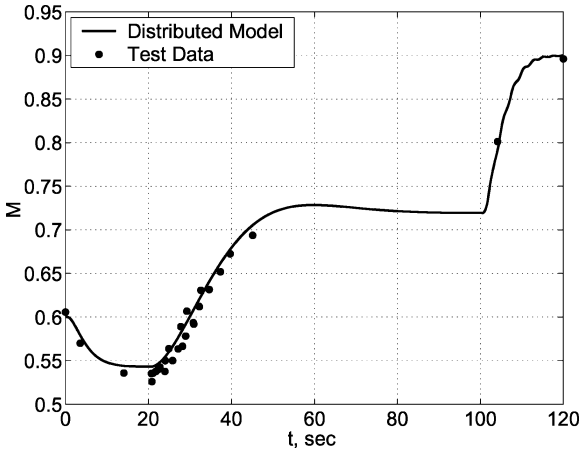


**Fig. 5 Mach number response.**

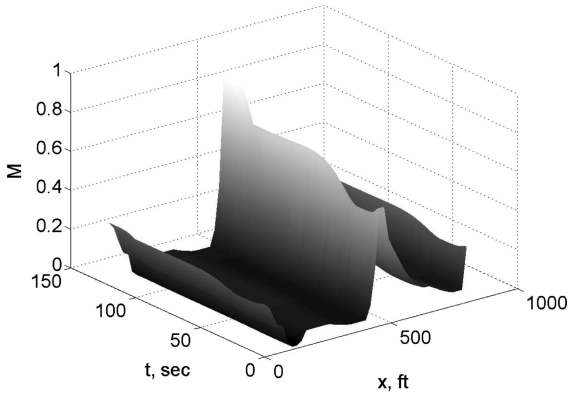


**Fig. 6 Mach number distribution.**

With reference to Fig. 4, the IGV flap deflection is first adjusted to its maximum value while the compressor speed is regulated at 455 rpm. A new compressor speed set-point command at 590 rpm is then sought while the IGV flap deflection is maintained at its maximum value. When the compressor settles to the new set point, the IGV flaps are then actuated until the Mach number reaches 0.9. A small ripple in the compressor speed occurs at the beginning of the final IGV flap actuation because of the an integral feedback control regulating the motor-speed set point as a result of the changing aerodynamic torque during the IGV actuation.

Figure 5 shows the resulting Mach number variation throughout the transition. The computed Mach number from the distributed model agrees very well with the experimental data. It is noted that the sequential mode of setting the Mach number using either the compressor speed or the IGV flap deflection is by design due to the lack of an interaction model between the compressor speed and the IGV flap deflection in the current control algorithm. This shortcoming is overcome with the proposed model as presented.

Figure 6 is the plot of the Mach number distribution along the wind tunnel that illustrates the distributed nature of the wind-tunnel model. The flow variables in the test section are dependent continuously on the flow variables throughout the wind tunnel.

The accuracy of the wind-tunnel distributed model as demonstrated provides a basis on which the proposed predictive Mach number optimal control is to be designed. Toward that end, optimal control of a distributed system modeled by PDEs coupled with an ODE lumped-parameter system is a new subject area that has not been fully investigated. This paper, therefore, will examine the optimality conditions of such a system in the context of an adjoint formulation based on calculus of variations. These optimality conditions will then be used to establish the predictive Mach number optimal control with a linear-quadratic cost function for the wind tunnel.

## Optimality Conditions

To derive the optimality conditions, we consider the following general cost function with a free final time $t_f$:

$$J = \int_0^{t_f} \int_0^L L_1(\boldsymbol{y}, x)dxdt + \int_0^{t_f} L_2[\boldsymbol{y}(0,t), \boldsymbol{y}(L,t), \boldsymbol{u}, \boldsymbol{v}]dt \tag{10}$$

subject to a distributed system (S) and a lumped-parameter system (P) to be defined as follows: The distributed system (S) is governed by a system of first-order hyperbolic PDEs,

$$\boldsymbol{y}_t + \boldsymbol{A}(\boldsymbol{y}, x)\boldsymbol{y}_x + \boldsymbol{B}(\boldsymbol{y}, x) = \boldsymbol{0} \qquad \forall x \in (0, L), t \in (0, t_f) \tag{11}$$

where $\boldsymbol{y}(x,t) : (0,L) \times (0,t_f) \to \mathbb{R}^n$ is a distributed state vector, $\boldsymbol{A}(\boldsymbol{y}, x) : \mathbb{R}^n \times (0,L) \to \mathbb{R}^n \times \mathbb{R}^n$ is a square characteristic matrix, and $\boldsymbol{B}(\boldsymbol{y}, x) : \mathbb{R}^n \times (0,L) \to \mathbb{R}^n$ is a source vector.

We make the important assumption that $\boldsymbol{y}(x,t)$ admits only continuous solutions because it is well known that hyperbolic equations can also admit discontinuous solutions known as entropy solutions.[9]

The system (S) is said to be strictly hyperbolic if the matrix $\boldsymbol{A}$ has $n$ real, distinct eigenvalues such that $\lambda_1(\boldsymbol{A}) < \lambda_2(\boldsymbol{A}) < \cdots \lambda_n(\boldsymbol{A})$ for all $\boldsymbol{y}(x,t) \in \mathbb{R}^n$. Thus, $\boldsymbol{A}$ is a diagonalizable matrix.

A two-point boundary condition is imposed on the system (S) as follows:

$$\boldsymbol{y}(0,t) = \boldsymbol{g}(\boldsymbol{y}(L,t), \boldsymbol{u}) \qquad \forall t \in (0, t_f) \tag{12}$$

where $\boldsymbol{u}(t) : (0,t_f) \to \mathbb{R}^m$ is a lumped-parameter state vector, and $\boldsymbol{g}[\boldsymbol{y}(L,t), \boldsymbol{u}] : \mathbb{R}^n \times \mathbb{R}^m \to \mathbb{R}^n$ is a vector function that satisfies a well-posedness requirement; that is, $\dim[\boldsymbol{g}_{y(L,t)}] \geq n^-$ where $n^-$ is the number of negative eigenvalues.

The following initial condition is specified:

$$\boldsymbol{y}(x,0) = \boldsymbol{y}_0(x) \qquad \forall x \in (0, L) \tag{13}$$

The compatibility between the boundary condition and initial condition requires that

$$\boldsymbol{y}_0(0) = \boldsymbol{g}[\boldsymbol{y}(L,0), \boldsymbol{u}(0)] \tag{14}$$

The lumped-parameter system (P) controls the distributed system (S) via the boundary condition in Eq. (12) as

$$\dot{\boldsymbol{u}} = \boldsymbol{f}[\boldsymbol{y}(0,t), \boldsymbol{y}(L,t), \boldsymbol{u}, \boldsymbol{v}] \qquad \forall t \in (0, t_f) \tag{15}$$

where $\boldsymbol{v}(t) : (0,t_f) \to \mathbb{R}^l$ belong to a convex subset of admissible control $\mathcal{V}_{ad} \subseteq \mathbb{R}^l$, and $\boldsymbol{f}[\boldsymbol{y}(0,t), \boldsymbol{y}(L,t), \boldsymbol{u}, \boldsymbol{v}] : \mathbb{R}^n \times \mathbb{R}^n \times \mathbb{R}^k \times \mathbb{R}^l \to \mathbb{R}^k$ is a transition vector function.

The following initial condition for the system (P) is specified:

$$\boldsymbol{u}(0) = \boldsymbol{u}_0 \tag{16}$$

For compactness, let $\boldsymbol{y}^0(t) = \boldsymbol{y}(0,t)$ and $\boldsymbol{y}^L(t) = \boldsymbol{y}(L,t)$ with the superscripts 0 and $L$ henceforth meaning the values at $x = 0$ and $x = L$. We assume that $\boldsymbol{v}(t)$ is an unbounded control that is measurable and squared-integrable with $L^2$ norms bounded on $(0, t_f)$.

To define the optimality conditions, we introduce a dual Hamiltonian system for the systems (S) and (P) as

$$H_1(\boldsymbol{y}, \boldsymbol{\lambda}, x) = L_1 - \boldsymbol{\lambda}^T \boldsymbol{B} \tag{17}$$

$$H_2(\boldsymbol{y}^0, \boldsymbol{y}^L, \boldsymbol{u}, \boldsymbol{v}, \boldsymbol{\mu}, \boldsymbol{\eta}) = H_3 + \boldsymbol{\eta}^T(\boldsymbol{g} - \boldsymbol{y}^0) \tag{18}$$

where $\boldsymbol{\lambda}(x,t) : (0,L) \times (0,t_f) \to \mathbb{R}^n$ is the adjoint vector for the system (S), $\boldsymbol{\eta}(t) : (0,t_f) \to \mathbb{R}^n$ is the adjoint vector for the boundary condition, and $H_3$ is the customary Hamiltonian function for the system (P) defined without the boundary condition as

$$H_3(\boldsymbol{y}^0, \boldsymbol{y}^L, \boldsymbol{u}, \boldsymbol{v}, \boldsymbol{\mu}) = L_2 + \boldsymbol{\mu}^T \boldsymbol{f} \tag{19}$$

where $\boldsymbol{\mu}(t) : (0,t_f) \to \mathbb{R}^m$ is the adjoint vector for the system (P).

Applying the Lagrange multiplier yields the following augmented cost function:

$$J = \int_0^{t_f}\int_0^{L}\left[H_1 - \boldsymbol{\lambda}^T(\boldsymbol{y}_t + \boldsymbol{A}\boldsymbol{y}_x)\right]dxdt + \int_0^{t_f}\left(H_2 - \boldsymbol{\mu}^T\dot{\boldsymbol{u}}\right)dt \quad (20)$$

The first variation of the cost function $J$ is computed as

$$\begin{aligned}\delta J = &\int_0^{t_f}\int_0^{L}\left[H_{1,y}\delta\boldsymbol{y} - \boldsymbol{\lambda}^T(\delta\boldsymbol{y}_t + \boldsymbol{A}\delta\boldsymbol{y}_x + \boldsymbol{A}_y\boldsymbol{y}_x\delta\boldsymbol{y})\right]dxdt\\ &+ \int_0^{t_f}\left(H_{2,y^0}\delta\boldsymbol{y}^0 + H_{2,y^L}\delta\boldsymbol{y}^L + H_{2,u}\delta\boldsymbol{u} + H_{2,v}\delta\boldsymbol{v} - \boldsymbol{\mu}^T\delta\dot{\boldsymbol{u}}\right)dt\\ &+ \int_0^{L}\left[H_1 - \boldsymbol{\lambda}^T(\boldsymbol{y}_t + \boldsymbol{A}\boldsymbol{y}_x)\right]_{t=t_f}\delta t dx + \left(H_2 - \boldsymbol{\mu}^T\dot{\boldsymbol{u}}\right)_{t=t_f}\delta t\end{aligned} \quad (21)$$

When we invoke the Green's theorem, the equation yields

$$\begin{aligned}&\int\int\boldsymbol{\lambda}^T(\delta\boldsymbol{y}_t + \boldsymbol{A}\delta\boldsymbol{y}_x + \boldsymbol{A}_y\boldsymbol{y}_x\delta\boldsymbol{y})dxdt\\ &\quad = -\int\int\left(\boldsymbol{\lambda}_t^T + \boldsymbol{\lambda}_x^T\boldsymbol{A} + \boldsymbol{\lambda}^T\boldsymbol{A}_x\right)\delta\boldsymbol{y}dxdt + b\end{aligned} \quad (22)$$

where the boundary condition term $b$ is given as

$$b = \int_0^{t_f}\left[(\boldsymbol{\lambda}^L)^T\boldsymbol{A}^L\delta\boldsymbol{y}^L - (\boldsymbol{\lambda}^0)^T\boldsymbol{A}^0\delta\boldsymbol{y}^0\right]dt + \int_0^{L}\boldsymbol{\lambda}^T\delta\boldsymbol{y}\Big|_{t=t_f}dx \quad (23)$$

When we use the foregoing results, the first variation of the cost function $J$ becomes

$$\begin{aligned}\delta J = &\int_0^{t_f}\int_0^{L}\left(H_{1,y} + \boldsymbol{\lambda}_t^T + \boldsymbol{\lambda}_x^T\boldsymbol{A} + \boldsymbol{\lambda}^T\boldsymbol{A}_x\right)\delta\boldsymbol{y}dxdt\\ &+ \int_0^{L}\left[H_1 - \boldsymbol{\lambda}^T(\boldsymbol{y}_t + \boldsymbol{A}\boldsymbol{y}_x)\right]_{t=t_f}\delta t dx\\ &- \int_0^{t_f}\left[(\boldsymbol{\lambda}^L)^T\boldsymbol{A}^L\delta\boldsymbol{y}^L - (\boldsymbol{\lambda}^0)^T\boldsymbol{A}^0\delta\boldsymbol{y}^0\right]dt\\ &- \int_0^{L}\boldsymbol{\lambda}^T\delta\boldsymbol{y}\Big|_{t=t_f}dx - \boldsymbol{\mu}^T\delta\boldsymbol{u}\Big|_{t=t_f}\\ &+ \int_0^{t_f}\left(H_{2,y^0}\delta\boldsymbol{y}^0 + H_{2,y^L}\delta\boldsymbol{y}^L + H_{2,u}\delta\boldsymbol{u} + H_{2,v}\delta\boldsymbol{v} - \dot{\boldsymbol{\mu}}^T\delta\boldsymbol{u}\right)dt\\ &+ \left(H_2 - \boldsymbol{\mu}^T\dot{\boldsymbol{u}}\right)_{t=t_f}\delta t\end{aligned} \quad (24)$$

A necessary optimality condition for a relative minimum of the cost function $J$ requires that the first variation be zero for any arbitrary admissible variation. As a result, the following associated distributed adjoint system ($\Sigma$) and lumped-parameter adjoint system ($\Pi$) are obtained:

$$\boldsymbol{\lambda}_t + \boldsymbol{A}^T\boldsymbol{\lambda}_x + \boldsymbol{A}_x^T\boldsymbol{\lambda} + H_{1,y}^T = \boldsymbol{0} \quad (25)$$

$$\dot{\boldsymbol{\mu}} = -H_{2,u}^T \quad (26)$$

The necessary optimality condition for an unbounded optimal control of the system (P) is given by

$$H_{2,v}^T = \boldsymbol{0} \quad (27)$$

In addition, two auxiliary algebraic equations are also obtained:

$$(\boldsymbol{A}^0)^T\boldsymbol{\lambda}^0 + H_{2,y^0}^T = \boldsymbol{0} \quad (28)$$

$$(\boldsymbol{A}^L)^T\boldsymbol{\lambda}^L - H_{2,y^L}^T = \boldsymbol{0} \quad (29)$$

When we solve for the adjoint vectors $\boldsymbol{\eta}(t)$ from Eq. (28) in terms of the Hamiltonian function $H_3$, the math yields

$$\boldsymbol{\eta} = (\boldsymbol{A}^0)^T\boldsymbol{\lambda}^0 + H_{3,y^0}^T$$

Upon substitution, the following boundary condition for the adjoint system ($\Sigma$) is obtained:

$$(\boldsymbol{A}^L)^T\boldsymbol{\lambda}^L = H_{3,y^L}^T + \boldsymbol{g}_{y^L}^T(\boldsymbol{A}^0)^T\boldsymbol{\lambda}^0 + \boldsymbol{g}_{y^L}^T H_{3,y^0}^T \quad (30)$$

From the foregoing results, the adjoint system ($\Pi$) in terms of the Hamiltonian function $H_3$ may be expressed as

$$\dot{\boldsymbol{\mu}} = -H_{3,u}^T - \boldsymbol{g}_u^T(\boldsymbol{A}^0)^T\boldsymbol{\lambda}^0 - \boldsymbol{g}_u^T H_{3,y^0}^T \quad (31)$$

The associated transversality conditions for the adjoint systems ($\Sigma$) and ($\Pi$) are as follows:

$$\boldsymbol{\lambda}^T(x, t_f)\delta\boldsymbol{y}(x, t_f) = 0 \quad (32)$$

$$\boldsymbol{\mu}^T(t_f)\delta\boldsymbol{u}(t_f) = 0 \quad (33)$$

In addition to the foregoing optimality conditions, we also have a final-time condition that allows the free final time $t_f$ to be determined:

$$\int_0^{L}\left[H_1 - \boldsymbol{\lambda}^T(\boldsymbol{y}_t + \boldsymbol{A}\boldsymbol{y}_x)\right]_{t=t_f}dx + \left(H_2 - \boldsymbol{\mu}^T\dot{\boldsymbol{u}}\right)_{t=t_f} = 0 \quad (34)$$

If the final-time conditions for $\boldsymbol{y}(x, t)$ and $\boldsymbol{u}(t)$ are unspecified, then the transversality conditions require that the adjoint vectors $\boldsymbol{\lambda}(x, t)$ and $\boldsymbol{\mu}(t)$ be zero. The final-time condition is then reduced to

$$\int_0^{L}H_1|_{t=t_f}dx + H_2|_{t=t_f} = 0 \quad (35)$$

It can be seen that the optimal-control vector $\boldsymbol{v}(t)$ depends not only on the adjoint vector $\boldsymbol{\mu}(t)$ but also on the adjoint vectors $\boldsymbol{\lambda}(0, t)$ and $\boldsymbol{\lambda}(L, t)$ at the boundaries of the system ($\Sigma$). Generally, the optimal control can be computed in a open loop as a function of time by solving two sets of two-point boundary-value PDE and ODE problems simultaneously. When we obtain $\boldsymbol{v}(t)$, the state vector $\boldsymbol{u}(t)$ is computed by integrating Eq. (15) forward in time. Equation (11) can then be integrated forward in space and time to compute the optimal trajectory of the distributed state vector $\boldsymbol{y}(x, t)$ of the system (S).

## Linear-Quadratic Optimal Control

We now apply the general theory that has been developed to design a state feedback optimal control for the following linear hyperbolic equation:

$$\frac{1}{\alpha(x)}\frac{\partial y}{\partial t} + \frac{\partial y}{\partial x} + \beta(x, t)y + w(t) = 0 \quad (36)$$

subject to the boundary condition

$$y(0, t) = \boldsymbol{G}\boldsymbol{u}(t) + Hy(L, t) \quad (37)$$

and an initial condition

$$y(x, 0) = 0 \quad (38)$$

Equation (36) is sometimes referred to as a linear advection equation and is typically used in modeling transport phenomena such as fluid flow or traffic flow. The term $w(t)$ represents a disturbance to the hyperbolic system.

The lumped-parameter state equation is defined as

$$\dot{\boldsymbol{u}} = \boldsymbol{C}\boldsymbol{u} + \boldsymbol{D}\boldsymbol{v} + \boldsymbol{E}y(0, t) + \boldsymbol{F}y(L, t) \quad (39)$$

subject to a compatible initial condition,

$$\boldsymbol{u}(0) = \boldsymbol{0} \quad (40)$$

To design a feedback optimal control, we consider the following linear-quadratic cost function with a fixed final time $t_f$:

$$J = \int_0^{t_f} \left[ \frac{1}{2} P y^2(0,t) + \frac{1}{2} \boldsymbol{u}^T \boldsymbol{Q} \boldsymbol{u} + \frac{1}{2} \boldsymbol{v}^T \boldsymbol{R} \boldsymbol{v} \right] dt \tag{41}$$

where $P \geq 0$, $\boldsymbol{Q} \geq \boldsymbol{0}$, and $\boldsymbol{R} > \boldsymbol{0}$.

We define the following Hamiltonian functions:

$$H_1 = -\lambda\alpha(\beta y + w) \tag{42}$$

$$H_3 = \tfrac{1}{2} P y^2(0,t) + \tfrac{1}{2} \boldsymbol{u}^T \boldsymbol{Q} \boldsymbol{u} + \tfrac{1}{2} \boldsymbol{v}^T \boldsymbol{R} \boldsymbol{v} + \boldsymbol{\mu}^T [\boldsymbol{C}\boldsymbol{u} + \boldsymbol{D}\boldsymbol{v} + \boldsymbol{E} y(0,t) + \boldsymbol{F} y(L,t)] \tag{43}$$

The optimality conditions as derived result in the following equations:

$$\frac{\partial \lambda}{\partial t} + \frac{\partial}{\partial x}(\alpha\lambda) - \beta\alpha\lambda = 0 \tag{44}$$

$$\alpha(L)\lambda(L,t) = H\alpha(0)\lambda(0,t) + H P y(0,t) + (\boldsymbol{F}^T + H\boldsymbol{E}^T)\boldsymbol{\mu} \tag{45}$$

$$\alpha(x)\lambda(x,t_f) = 0 \tag{46}$$

$$\dot{\boldsymbol{\mu}} = -\boldsymbol{Q}\boldsymbol{u} - (\boldsymbol{C}^T + \boldsymbol{G}^T\boldsymbol{E}^T)\boldsymbol{\mu} - \boldsymbol{G}^T\alpha(0)\lambda(0,t) - \boldsymbol{G}^T P y(0,t) \tag{47}$$

$$\boldsymbol{\mu}(t_f) = 0 \tag{48}$$

$$\boldsymbol{R}\boldsymbol{v} + \boldsymbol{D}^T\boldsymbol{\mu} = 0 \tag{49}$$

These equations, along with Eqs. (36–40), form a two-point boundary value PDE–ODE problem. Even though they are linear, the two-point boundary conditions in Eqs. (37) and (45) pose a challenge in obtaining a general feedback control solution. One obvious solution is to solve this problem directly using any numerical optimization technique such as a gradient method, but that would render the optimal control as an open-loop process.

To understand the challenge, we examine the nature of the solution of Eq. (36). The characteristic method can be used to solve a linear advection hyperbolic PDE by converting it into an ODE along a characteristic direction in the $(x,t)$ plane defined by

$$\frac{dx}{dt} = \alpha(x) \tag{50}$$

Then, it can be shown that the general solution of Eq. (36) is

$$y(x,t) = a(x,t)\{f[t - t_d(x)] - q(x,t)\} \tag{51}$$

where

$$t_d(x) = \int_0^x \frac{d\sigma}{\alpha(\sigma)} \tag{52}$$

$$a(x,t) = \exp\left\{ -\int_0^x \beta[\sigma, t - t_d(x) + t_d(\sigma)] d\sigma \right\} \tag{53}$$

$$q(x,t) = \int_0^x a^{-1}[\sigma, t - t_d(x) + t_d(\sigma)] w[t - t_d(x) + t_d(\sigma)] d\sigma \tag{54}$$

We see that the general solution involves a variable time delay $t_d(x)$, which is a characteristic of a hyperbolic system. The function $q(x,t)$ is the forcing function term resulting from the disturbance, whereas the function $f[t - t_d(x)]$ represents the effect of the wave propagation and must be determined from the boundary condition in Eq. (37) as

$$y(0,t) = f(t) = \boldsymbol{G}\boldsymbol{u}(t) + Ha(L,t)\{f[t - t_d(L)] - q(L,t)\} \tag{55}$$

To solve for Eq. (55), we recognize that $f[t - t_d(L)] = 0$ for $t < t_d(L)$ because of the zero initial condition. Let $t_L = t_d(L)$; then, the solution is found to be

$$y(0,t) = f(t) = \boldsymbol{G}\boldsymbol{u}(t) + \sum_{k=1}^{n} \left[ \prod_{m=0}^{k-1} Ha(L, t - mt_L) \right] \boldsymbol{G}\boldsymbol{u}(t - kt_L) - \sum_{k=0}^{n} \left[ \prod_{m=0}^{k} Ha(L, t - mt_L) \right] q(L, t - kt_L) \tag{56}$$

To solve for the adjoint PDE from Eq. (44), we first perform a time and space reversal coordinate transformation by letting $z(\chi,\tau) = \alpha(x)\lambda(x,t)$ where $\chi = L - x$ is the distance to go and $\tau = t_f - t$ is the time to go. Then, the general solution of the adjoint variable is obtained as

$$z(\chi,\tau) = b(\chi,\tau) g[\tau - \tau_d(\chi)] \tag{57}$$

where

$$\tau_d(\chi) = \int_0^{\chi} \frac{d\sigma}{\alpha(L - \sigma)} = t_L - t_d(x) \tag{58}$$

$$b(\chi,\tau) = \exp\left\{ -\int_0^{\chi} \beta[L - \sigma, t_f - \tau + \tau_d(\chi) - \tau_d(\sigma)] d\sigma \right\} = a(L,t) a^{-1}(x,t) \tag{59}$$

When we apply the boundary condition from Eq. (45) to solve for the wave propagation function $g[\tau - \tau_d(\chi)]$, we get

$$g(\tau) = Hc(L,\tau) g(\tau - t_L) + H P y(0, t_f - \tau) + (\boldsymbol{F}^T + H\boldsymbol{E}^T)\boldsymbol{\mu}(t_f - \tau) \tag{60}$$

From the transversality condition, we recognize that $g(\tau - t_L) = 0$ for $\tau < t_L$. This then gives the following solution:

$$\begin{aligned} g(\tau) = {} & H P y(0, t_f - \tau) + \sum_{k=1}^{n} \left[ \prod_{m=0}^{k-1} Hb(L, \tau - mt_L) \right] \\ & \times H P y(0, t_f - \tau + kt_L) + (\boldsymbol{F}^T + H\boldsymbol{E}^T)\boldsymbol{\mu}(t_f - \tau) \\ & + \sum_{k=1}^{n} \left[ \prod_{m=0}^{k-1} Hb(L, \tau - mt_L) \right] (\boldsymbol{F}^T + H\boldsymbol{E}^T)\boldsymbol{\mu}(t_f - \tau + kt_L) \end{aligned} \tag{61}$$

By transforming from the $(\chi,\tau)$ coordinates to the $(x,t)$ coordinates, we obtain the solution of the adjoint as

$$\begin{aligned} \alpha(0)\lambda(0,t) = {} & Ha(L,t) P y(0, t + t_L) \\ & + (\boldsymbol{F}^T + H\boldsymbol{E}^T)\, a(L,t)\boldsymbol{\mu}(t + t_L) \\ & + \sum_{k=1}^{n} \left[ \prod_{m=0}^{k-1} Ha(L, t + mt_L) \right] Ha(L,t) P y[0, t + (k+1)t_L] \\ & + \sum_{k=1}^{n} \left[ \prod_{m=0}^{k-1} Ha(L, t + mt_L) \right] \\ & \times (\boldsymbol{F}^T + H\boldsymbol{E}^T)\, a(L,t)\boldsymbol{\mu}[t + (k+1)t_L] \end{aligned} \tag{62}$$

We note that the adjoint solution $\alpha(0)\lambda(0,t)$ depends on future values of $y(0,t)$ and $\boldsymbol{\mu}(t)$, whereas the solution of $y(0,t)$ depends on past values of $\boldsymbol{u}(t)$ and $q(L,t)$. The time-shifted nature of this two-point boundary-value problem illustrates the challenge with the optimal-control solution even though the system is linear. For a practical control application, we now introduce a simplified solution method for this two-point boundary-value problem in the limit.

We consider two special cases: one for $t_f < t_L$ and the other for $t_f \to \infty$. In the first case, the system is noncausal; that is, it depends on future information that is not yet available. Therefore, to enforce

the causality, $\alpha(0)\lambda(0,t)$ must be zero. Thus, for a short time horizon when $t_f < t_L$, we have the following relationship:

$$y(0,t) = \boldsymbol{G}\boldsymbol{u}(t) - Ha(L,t)q(L,t) \tag{63}$$

$$y(L,t) = -a(L,t)q(L,t) \tag{64}$$

$$\alpha(0)\lambda(0,t) = 0 \tag{65}$$

However, for a long time horizon when $t_f \to \infty$ and the system is stabilizing, we have $f(t-t_L) \simeq f(t)$ and $g(\tau - t_L) \simeq g(\tau)$. We then obtain from Eqs. (55) and (60)

$$y(0,t) = [1 - Ha(L,t)]^{-1}[\boldsymbol{G}\boldsymbol{u}(t) - Ha(L,t)q(L,t)] \tag{66}$$

$$y(L,t) = a(L,t)[1 - Ha(L,t)]^{-1}[\boldsymbol{G}\boldsymbol{u}(t) - Ha(L,t)q(L,t)] - a(L,t)q(L,t) \tag{67}$$

$$\alpha(0)\lambda(0,t) = a(L,t)[1 - Ha(L,t)]^{-1}[HPy(0,t) + (\boldsymbol{F}^T + H\boldsymbol{E}^T)\boldsymbol{\mu}(t)] \tag{68}$$

By substituting these results into Eqs. (39) and (47), we obtain the following Hamiltonian system:

$$\begin{bmatrix}\dot{\boldsymbol{u}}\\ \dot{\boldsymbol{\mu}}\end{bmatrix} = \begin{bmatrix}\boldsymbol{C}_e & -\boldsymbol{D}\boldsymbol{R}^{-1}\boldsymbol{D}^T\\ -\boldsymbol{Q}_e & -\boldsymbol{C}_e^T\end{bmatrix}\begin{bmatrix}\boldsymbol{u}\\ \boldsymbol{\mu}\end{bmatrix} + \begin{bmatrix}-\boldsymbol{S}\\ \boldsymbol{U}\end{bmatrix} \tag{69}$$

where

$$\boldsymbol{C}_e = \boldsymbol{C} + \boldsymbol{E}\boldsymbol{G} + \gamma(\boldsymbol{F} + \boldsymbol{E}H)\boldsymbol{G}a(L,t)[1 - \gamma Ha(L,t)]^{-1} \tag{70}$$

$$\boldsymbol{Q}_e = \boldsymbol{Q} + \boldsymbol{G}^T P\boldsymbol{G}[1 - \gamma Ha(L,t)]^{-2} \tag{71}$$

$$\boldsymbol{S} = (\boldsymbol{F} + \boldsymbol{E}H)a(L,t)q(L,t)[1 - \gamma Ha(L,t)]^{-1} \tag{72}$$

$$\boldsymbol{U} = \boldsymbol{G}^T PHa(L,t)q(L,t)[1 - \gamma Ha(L,t)]^{-2} \tag{73}$$

The parameter $\gamma$ takes on a value ranging from 0 to 1 that represents the effect of the time horizon on the optimal-control solution such that $\gamma = 0$ corresponds to a short time horizon and $\gamma = 1$ corresponds to a long time horizon. The solution of a Hamiltonian system is well known and involves the Riccati equation using a backward sweep method by letting $\boldsymbol{\mu} = \boldsymbol{W}\boldsymbol{u} + \boldsymbol{V}$ where

$$\dot{\boldsymbol{W}} + \boldsymbol{W}\boldsymbol{C}_e + \boldsymbol{C}_e^T\boldsymbol{W} - \boldsymbol{W}\boldsymbol{D}\boldsymbol{R}^{-1}\boldsymbol{D}^T\boldsymbol{W} + \boldsymbol{Q}_e = \boldsymbol{0} \tag{74}$$

$$\dot{\boldsymbol{V}} + \boldsymbol{C}_e^T\boldsymbol{V} - \boldsymbol{W}\boldsymbol{D}\boldsymbol{R}^{-1}\boldsymbol{D}^T\boldsymbol{V} - \boldsymbol{W}\boldsymbol{S} - \boldsymbol{U} = \boldsymbol{0} \tag{75}$$

subject to the final time conditions $\boldsymbol{W}(t_f) = \boldsymbol{0}$ and $\boldsymbol{V}(t_f) = \boldsymbol{0}$.

We have thus demonstrated that the optimal-control solution of a first-order hyperbolic equation coupled with an ODE system also has a Riccati solution. The distributed system matrices $\boldsymbol{E}$, $\boldsymbol{F}$, $\boldsymbol{G}$, and $H$ effectively modify the weighting matrix $\boldsymbol{Q}$ and dynamic matrix $\boldsymbol{C}$ of the lumped-parameter system. The optimal control $\boldsymbol{v}$ therefore is expressed as a state feedback control as

$$\boldsymbol{v}(t) = -\boldsymbol{R}^{-1}\boldsymbol{D}^T\boldsymbol{W}(t)\boldsymbol{u}(t) - \boldsymbol{R}^{-1}\boldsymbol{D}^T\boldsymbol{V}(t) \tag{76}$$

## Predictive Mach Number Optimal Control

The linear-quadratic optimal-control results can now be applied to design a predictive Mach number control for a wind tunnel. The objective of a wind-tunnel operation is to control and stabilize the Mach number in the test section resulting from a small total pressure disturbance created by the test-model drag as accurately as possible. We neglect the continuity and energy equations because the mass flow and total temperature are not very sensitive to the test-model drag-induced total pressure disturbance, and then linearize Eq. (4) about a steady-state nominal operating condition, which results in a linearized momentum equation expressed in the form of Eq. (36) with $y(x,t) = \Delta p_0(x,t)$ and various terms in that equation defined as

$$\alpha(x) = \bar{M}(x)\bar{c}(x)\frac{4 - 2k + (k-1)\bar{M}^2(x)}{2 + (k-1)\bar{M}^2(x)} \tag{77}$$

$$\beta(x,t) = -\frac{k\bar{M}^2(x)[1 + k\bar{M}^2(x)]}{2[1 - \bar{M}^2(x)]}\left[\frac{f(x)}{D(x)} + \frac{C_D(t)A_m}{A(x_t)L_m}\right] \tag{78}$$

$$w(t) = \frac{k}{2}\bar{p}_0(x_t)\bar{M}^2(x_t)\frac{C_D(t)A_m}{A(x_t)L_m} \tag{79}$$

where $M$ is the Mach number, $C_D$ is the test-model drag coefficients, $A_m$ and $L_m$ are the test-model reference area and length, $x_t$ is the coordinate of the test section, and the overbar denotes the steady-state condition.

The validity of this equation excludes the transonic region when $\bar{M}(x_t) \simeq 1$. Because we want to regulate the compressor speed at all times, the boundary condition in Eq. (37) is defined with $\boldsymbol{u} = [\Delta\theta \;\; \Delta\omega \;\; \xi]^T$ as a compressor state error vector comprising the IGV flap-deflection error $\Delta\theta$, the compressor-speed error $\Delta\omega$, and the compressor-speed error integral

$$\xi = \int_0^t \Delta\omega d\tau$$

The error integral is designed to ensure a zero steady-state error in the compressor speed. In essence, the control scheme is a proportional-integral control. The matrices

$$\boldsymbol{G} = \left[\frac{\partial p_0(0,t)}{\partial\theta} \quad \frac{\partial p_0(0,t)}{\partial\omega} \quad 0\right], \qquad H = \frac{\partial p_0(0,t)}{\partial p_0(L,t)}$$

are evaluated from Eq. (6). The compressor-state error dynamics is modeled by Eq. (39) with $\boldsymbol{v} = [\Delta V_a \;\; \Delta R_r]^T$ as a control vector comprising the corrective control inputs and the various matrices defined as

$$\boldsymbol{C} = \begin{bmatrix}\frac{\partial\dot{\theta}}{\partial\theta} & \frac{\partial\dot{\theta}}{\partial\omega} & 0\\ \frac{\partial\dot{\omega}}{\partial\theta} & \frac{\partial\dot{\omega}}{\partial\omega} & 0\\ 0 & 1 & 0\end{bmatrix}, \qquad \boldsymbol{D} = \begin{bmatrix}\frac{\partial\dot{\theta}}{\partial V} & 0\\ 0 & \frac{\partial\dot{\omega}}{\partial R_r}\\ 0 & 0\end{bmatrix}$$

$$\boldsymbol{E} = \begin{bmatrix}0\\ \frac{\partial\dot{\omega}}{\partial p_0(0,t)}\\ 0\end{bmatrix}, \qquad \boldsymbol{F} = \begin{bmatrix}\frac{\partial\dot{\theta}}{\partial p_0(L,t)}\\ \frac{\partial\dot{\omega}}{\partial p_0(L,t)}\\ 0\end{bmatrix}$$

The state feedback optimal control for handling the total pressure disturbance generated by a continuous pitch of the test model can be computed directly from Eq. (76). The corrective control inputs for the drive motors and the IGV system are then added to the steady-state control inputs at a nominal Mach number to give the total drive-motor and IGV system-control inputs

$$\begin{bmatrix}V_a(t)\\ R_r(t)\end{bmatrix} = \begin{bmatrix}\bar{V}_a\\ \bar{R}_r\end{bmatrix} + \begin{bmatrix}\Delta V_a(t)\\ \Delta R_r(t)\end{bmatrix} \tag{80}$$

However, we recognize that the compressor generally does not sense the effect of the total pressure-disturbance signal caused by a continuous pitch of the test model at the same time instance as the disturbance itself. Because of the fluid transport delay, there is a time lag between the test section and the compressor inlet such that the compressor dynamic response lags behind the total pressure disturbance in the test section by a time delay of $\Delta t_d = t_d(L) - t_d(x_t)$. This lag time generally will cause the Mach number to drop before

the drive-motor and IGV system-control inputs in Eq. (80) can correct for it. Thus, to account for this time delay, the drive-motor and IGV system-control inputs must precede the total pressure disturbance in the test section by the same time lag. In effect, the Mach number control is a predictive scheme, whereby the control inputs have to be computed from a reasonable estimation of the system dynamic states and total pressure disturbance prior to the start of a continuous pitch polar when the state error signals are not yet available. Therefore, the predictive Mach number optimal control is a feedforward, open-loop scheme. The overall drive motor and IGV system control inputs can be computed as

$$\begin{bmatrix} V_a(t) \\ R_r(t) \end{bmatrix} = \begin{bmatrix} \bar{V}_a \\ \bar{R}_r \end{bmatrix} + \begin{bmatrix} \Delta V_a(t+\Delta t_d) \\ \Delta R_r(t+\Delta t_d) \end{bmatrix} \tag{81}$$

To demonstrate the effectiveness of the proposed predictive Mach number optimal control, we select a test section Mach number $\bar{M}(x_t) = 0.6$, a test section total pressure $\bar{p}_0(x_t) = 2116$ psf, and a ramp disturbance input of the test-model drag-induced parameter $[C_D A_m]/A_t = 0.0253$ from 0 to 15 s. The compressor speed is nominally at 455 rpm and the IGV flap deflection is at 11.5 deg. The geometry information is taken from the NASA Ames 11-ft TWT with a length $L = 795$ ft and the test section at $x_t = 470$ ft. The period is computed to be $t_L = 15.6$ s, and the time delay between the test section and the compressor inlet is computed to be $\Delta t_d = 3.6$ s. The system matrices are $\boldsymbol{G} = [-684.50 \;\; 25.542 \;\; 0]$, $H = 1.6013$, and

$$\boldsymbol{C} = \begin{bmatrix} -1.3565 \times 10^{-5} & 0 & 0 \\ 1.3223 & -0.059709 & 0 \\ 0 & 1 & 0 \end{bmatrix}$$

$$\boldsymbol{D} = \begin{bmatrix} 7.6358 \times 10^{-5} & 0 \\ 0 & -0.32543 \\ 0 & 0 \end{bmatrix}$$

$$\boldsymbol{E} = \begin{bmatrix} 0 \\ -0.0019318 \\ 0 \end{bmatrix}, \qquad \boldsymbol{F} = \begin{bmatrix} 3.1673 \times 10^{-9} \\ -0.0011615 \\ 0 \end{bmatrix}$$

The weighting matrices are selected to be $P = 0.001$, $Q_{22} = Q_{33} = 0.01$, $Q_{ij} = 0$ otherwise, $R_{11} = 1 \times 10^{-6}$, $R_{22} = 1$, and $R_{ij} = 0$ otherwise.

The results of the control simulation are presented in Figs. 7–10. Figure 7 is a plot of the feedback control inputs from Eq. (80) for the drive motors and the IGV system that show the effect of fluid transport delay in the first 3-s duration when the control inputs are essentially zero. The feedforward scheme from Eq. (81) in effect is designed to remove this time delay in the control inputs.

With reference to Fig. 8, the test-section Mach number responses for various control schemes are computed from the fully nonlinear model according to Eqs. (4–9). The feedback control schemes for

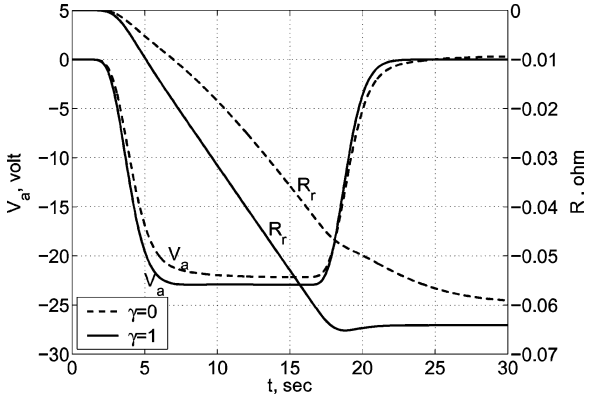


**Fig. 7 Feedback control.**

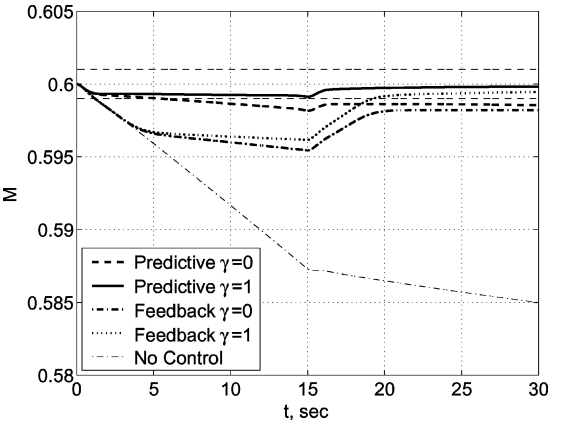


**Fig. 8 Mach number response.**

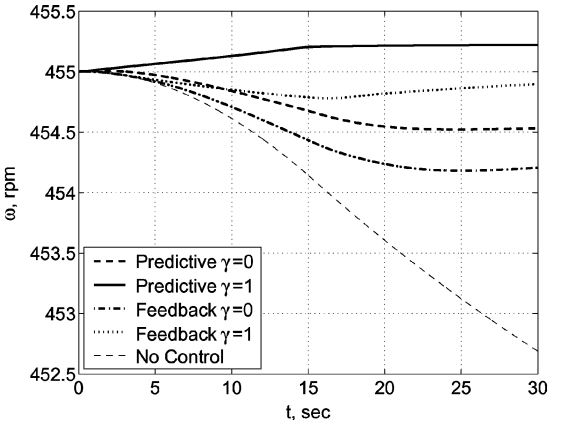


**Fig. 9 Compressor speed response.**

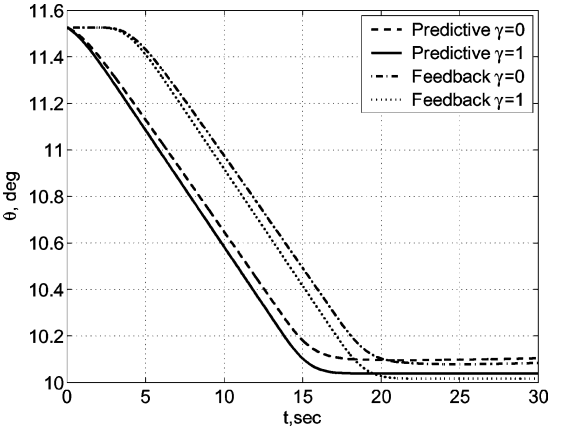


**Fig. 10 IGV flap-deflection response.**

both $\gamma = 0$ and $\gamma = 1$ clearly are not able to maintain the Mach number to within the tolerance band during the disturbance generated by the continuous pitch of the test model in the first 15 s. Because of the time delay during which the feedback control inputs are inactive as seen in Fig. 7, the Mach number drops below the tolerance band before the state error signals become available from the sensors at the compressor to allow the feedback control inputs to be computed. Once the feedback control inputs are applied to the drive motors and the IGV system, the Mach number begins to stabilize while the total pressure disturbance continues to increase to a maximum value at $t = 15$ s and is constant thereafter. The feedback control inputs then begin to cause the Mach number to return to its desired set point as time increases.

In contrast, the predictive feedforward control schemes for both $\gamma = 0$ and $\gamma = 1$ apparently are more effective in handling the total pressure disturbance. The predictive feedforward control scheme

for $\gamma = 0$ is an improving control relative to the feedback control schemes because it reduces the deviation in the Mach number but only can hold the Mach number for a very short time initially. In contrast, the predictive feedforward control scheme for $\gamma = 1$ is able to hold the Mach number to well within the tolerance band throughout the time horizon. This clearly demonstrates the effect of the time horizon parameter $\gamma$, which indicates that the predictive feedforward control scheme for a short time horizon is less effective than that for a long time horizon. We also note that if there were no corrective control, the Mach number would have dropped precipitously to 0.585 after 30 s.

Figure 9 shows the compressor speed responses to various control schemes. Both the predictive feedforward and feedback control schemes for $\gamma = 1$ are able to maintain the compressor speed reasonably well as compared to both the predictive feedforward and feedback control schemes for $\gamma = 0$, which appear to suffer a poorer regulation because of insufficient integral control efforts. It is also noted that if there were no corrective control, the compressor speed would have dropped precipitously at a rate of about 0.1 rpm/s.

The IGV flap deflection responses are presented in Fig. 10. The differences between the predictive feedforward and feedback control schemes illustrate the effect of the time delay quite clearly. The IGV flap deflections for the feedback control schemes lag behind those for the predictive feedforward control schemes by the same time delay between the test section and the compressor inlet. This lag explains why the test section Mach number generally cannot be controlled with a feedback control scheme during a continuous pitch. By implementing a predictive feedforward control scheme, this lag is effectively eliminated, thereby enabling the Mach number set point to be maintained during a continuous pitch of the test model. Because the compressor speed is not sensitive to various control schemes, the IGV flap deflection has a pronounced effect on the response of the test section Mach number. Thus, in theory, the compressor speed could still be controlled in a feedback mode, but the IGV flap deflection in general must be controlled according to the predictive feedforward control law.

In general, the accuracy of a predictive control is predicated upon the goodness of the estimation of the disturbance. Any significant deviation from the planned trajectory of the disturbance will likely cause the Mach number to exceed the tolerance band. Thus, to implement a predictive control scheme, it is necessary to have a priori knowledge of the time variation of the total pressure disturbance. Because the total pressure disturbance is a function of the drag force on the test model, it may be readily estimated from aerodynamic force measurements.

During a pitch polar, the aerodynamic forces generally vary as functions of the pitch angle as well as the Mach number and the Reynolds number. A database of the aerodynamic forces can be established as a table-lookup process for various combinations of the Mach number, the Reynolds number, and the pitch angle. In lieu of the lookup table, the aerodynamic-force relationships can also be established via an estimation process such as a recursive least-square or a neural-network algorithm that provides a functional approximation of the aerodynamic-force dependency. Using the knowledge of the time response of the model support system, a trajectory of the total pressure-disturbance parameter $w(t)$ can then be predicted for a given pitch polar by the neural-network computation or a linear interpolation from the lookup table. The trajectory of the total pressure disturbance is then used to compute the corrective optimal-control inputs for the predictive-control scheme. Using the predictive results of the optimal control, the compressor control is switched to an open-loop mode and begins its actuation simultaneously with the model support system's motion. At the end of the actuation, the compressor control is switched back to a feedback mode. The predictive Mach number control scheme thus potentially offers a significant advantage over a conventional feedback approach, which has been unable to regulate the Mach number during a continuous pitch polar.

## Conclusions

This paper describes a new optimal-control approach for a distributed system governed by first-order hyperbolic partial-differential equations coupled with a lumped-parameter system that accurately models a closed-citcuit wind tunnel. A general theory has been developed to analyze an optimal-control problem of this class of system. The theory is applied to a predictive optimal-control design to regulate the test section Mach number during a continuous pitch motion of a test model. The predictive optimal control is found to have a modified Riccati solution. A control simulation has demonstrated the effectiveness of this predictive optimal control in maintaining the Mach number during a continuous pitch motion. Therefore, it potentially offers a much better disturbance rejection than a typical feedback control because of the accuracy of the distributed model.

## References

[1]Bayen, A. M., Raffard, R. L., and Tomlin, C. J., "Eulerian Network Model of Air Traffic Flow in Congested Area," *Proceeding of the American Control Conference*, Vol. 6, 2004, pp. 5520–5526.

[2]Fursikov, A. V., Gunzburger, M. D., and Hou, L. S., "Boundary Value Problems and Optimal Boundary Control for the Navier–Stokes System: The Two-Dimensional Case," *SIAM Journal on Control and Optimization*, Vol. 36, No. 3, 1998, pp. 852–894.

[3]Raymond, J. P., and Zidani, H., "Pontryagin's Principle for State-Constrained Control Problems Governed by Parabolic Equations with Unbounded Controls," *SIAM Journal on Control and Optimization*, Vol. 36, No. 6, 1998, pp. 1853–1879.

[4]Troltzsch, F., "On the Lagrange–Newton–SQP Method for the Optimal Control of Semilinear Parabolic Equations," *SIAM Journal on Control and Optimization*, Vol. 38, No. 1, 1999, pp. 294–312.

[5]Inman, D. J., "Modal Decoupling Conditions for Distributed Control of Flexible Structures," *Journal of Guidance and Control*, Vol. 7, No. 6, 1984, pp. 750–752.

[6]Soeterboek, R. A. M., Pels, A. F., Verbruggen, H. B., and van Langen, G. C. A., "A Predictive Controller for Mach Number in a Wind Tunnel," *IEEE Control Systems*, Vol. 11, No. 1, 1991, pp. 63–72.

[7]Shapiro, A. H., *The Dynamics and Thermodynamics of Compressible Fluid Flow*, Vol. 2, Ronald Press Company, New York, 1954, Chap. 24, pp. 972–987.

[8]Hirsh, C., *Numerical Computation of Internal and External Flows*, Vol. 1, Wiley, New York, 1988, Chap. 4, pp. 167–180.

[9]Ulrich, S., "A Note on the Uniqueness of Entropy Solutions to First Order Quasilinear Equations," *SIAM Journal on Control and Optimization*, Vol. 41, No. 3, 2002, pp. 740–797.